Exploring the convective grey zone with regional simulations of a cold air outbreak

Paul R. Field, Radmila Brožková, Ming Chen, Jimy Dudhia, Christine Lac, Tabito Hara, Rachel Honnert, Joe Olson, Pier Siebesma, Stephan de Roode, Lorenzo Tomassini, Adrian Hill , Ron McTagart-Cowan

Sat Jun 24 07:04:22 2017

paul.field@metoffice.gov.uk

Abstract

Cold air outbreaks can bring snow to populated areas and can affect aviation safety. Shortcomings in the representation of these phenomena in global and regional models are thought to be associated with large systematic cloud related radiative flux errors across many models. In this study, nine regional models have been used to simulate a cold air outbreak case at a range of grid spacings (1km to 16km) with convection represented explicitly or by a parametrization. Overall, there is more spread between model results for the simulations in which convection is parametrized when compared to simulations in which convection is represented explicitly. The quality of the simulations of both the stratocumulus and the convective regions of the domain are assessed with observational comparisons 24 hours into the simulation. The stratocumulus region is not well reproduced by the models, which tend to predict open cell convection with increasing resolution rather than stratocumulus. For the convective region the model spread reduces with increased resolution and there is some improvement in comparison to observations. Comparing models that have the same physical parametrizations or dynamical core suggest that both are important for accurately reproducing this case.

Keywords: grey zone, convection permitting models
25 November 2016

1 Introduction

Many operational centres are now making use of km-scale models to carry out numerical weather prediction (Mailhot et al. 2010, Brousseau et al. 2016, Clark et al. 2016). The models at these grid resolutions are considered to be convection permitting and generally do not use a convective parametrization. The difficulty facing these models is that, although they do explicitly convect, they are not at high enough resolution to accurately represent the full spectrum of convective motions (Bryan et al. 2003).

It has long been recognised that a given phenomenon is explicitly resolved for model resolutions much finer than the size lp of the phenomenon. Likewise, at resolutions much coarser than lp, the phenomenon becomes unresolved and its effect on the resolved large scale flow can only indirectly be represented through parameterizations. Consequently, around the scale lp there exists a range of model resolutions for which the phenomenon is only partly resolved. This range of resolutions is often referred to as the Grey Zone.

Current global NWP models typically do not yet include grey zone convection schemes. The companion intercomparison study with global NWP models suggests that conventional convection parameterisations remove atmospheric instability too easily and prevent models from resolving part of the vertical overturning explicitly even at high resolutions (Tomassini et al., 2017). Another important aspect in the context of the grey zone parameterisation problem is the issue of physical parameterisation interferences. The global model intercomparison shows that in the cold-air outbreak case convection and boundary layer parameterisations strongly interact, which makes it impossible to restrict the grey zone parameterisation problem only to the convection scheme. Indeed, many traditional convection parameterisations even include separate components, like shallow, mid-level, and deep convection schemes, which might reciprocally affect each other. Therefore a unified approach is needed when it comes to addressing scale-adaptivity in the convective grey zone. Moreover, the important role of ice-microphysical processes and related precipitation formation hamper an unambiguous assessment of the impact of model resolution on the simulated cloud and boundary layer structures in the cold air outbreak case.

At resolutions finer than 10 km, the scale depth of the atmosphere, convective overturning starts to become resolved. Convection is a truly multiscale phenomenon ranging from the deep convective towers of 10 km to the smallest turbulent eddies of a few mm at the Kolmogorov scale. Therefore, the Grey Zone of convection encompasses a wide range of scales, so that refining the resolution in the Grey Zone leads to an continuous enrichment of the resolved convective processes. The fundamental question is how to parameterize the unresolved part of the convection in the Grey Zone in such a way that a parameterization is aware of the resolution and the part of the convection that is resolved.

For resolutions finer than a few hundred meters this is realized through an eddy

diffusivity approach where the model resolution is used as a length scale in the eddy diffusivity coefficient. This classic Smagorinsky closure describes how the effect of the parameterized turbulent diffusion decreases with increasing resolution and is based on the selfsimilar energy cascade of three-dimensional turbulence in the inertial subrange of the convective boundary layer.

However, resolutions in the range between 500 meter and 5 km are outside the inertial subrange and consequently the classic Smagorinsky closure is not applicable anymore. The moist convective processes that operate at these resolutions are usually parameterized through convection parameterizations that in general do not have a scale aware formulation. Instead it is common practice for models operating in the convective Grey Zone to simply switch off the convection parameterization somewhere in the resolution range between 500m and 5 km.

Previous exploration of the grey zone has focused on deeper convection in the tropics. The CASCADE project included simulations at resolution of 40,12,4,1.5km over West Africa and the tropical pacific. Generally it was found for the West African land based simulations that coarse resolution (12km) with convection parametrization switched off produced a better timed diurnal behaviour and subsequently agreed better with satellite based radar (Stein et al. 2015) and radiative flux measurements (Pearson et al. 2014). These studies over land and another over the tropical Pacific (Holloway et al. 2012) concluded that the highest resolution simulations with convection explicitly resolved agreed best with observations. Similarly, Gao et al (2017) report improved representation of precipitation spatial distribution and timing in higher resolution (4km when compared to 12 and 36km). These results suggest that, at least for deep convection, we should expect better comparison to observations at higher resolution. For shallow convection the convective flows that develop in km-scale models are grid-scale dependent and under-resolved (Sakradzija et al. 2016) necessitating the implementation of stochastic treatment that modifies the resolved flows and aims to better represent higher order moments of the motions.

In order to accelerate research of model simulations of moist convection in the Grey Zone the Working Group of Numerical Experimentation (WGNE) in collaboration with GEWEX Global Atmospheric Systems Study panel (GASS) has initiated a Grey Zone project that aims to analyse and improve convection parameterizations that operate at resolutions in the Grey Zone. A cold air outbreak situation has been selected as a first case to explore the behaviour the convective parameterizations in the Grey Zone.

Correctly simulating cold air outbreaks is important for weather forecasting. From a regional perspective they tend to be multi day events that can bring snow to populated areas. Moreover, they are known to be associated with lightning that affects aviation safety (Wilkinson et al. 2013) and icing conditions that create hazards for marine vessels (Moore 2013). They are a challenge to km-scale models because the boundary layer is shallow, but the horizontal open and closed cell mesoscale structures associated with the cold air outbreak can

reach scales up to almost 100 km. The question is whether these observed mesoscale structures can be realistically reproduced by km-scale models. Shortcomings in the representation of cold air outbreaks in climate models have been identified as leading to systematic errors in liquid water and broadband fluxes (Bodas-Salcedo et al. 2014). These errors have implications for sea ice and the general circulation (Hwang and Frierson 2013).

The cold air outbreak weather situation is unique in that it mixes the difficulties inherent in resolving boundary layer, convective structures, microphysics and their interactions. This study uses a novel application of a wide range of different model resolutions in tandem with structural model changes controlled by switching convective parametrizations on or off to explore the ability of NWP models to provide robust forecasts across the edge of the convective grey zone. In this paper the following questions are asked. i) How well do km-scale regional models resolve and simulate the evolution of a cold air outbreak? ii) What is the effect of grid resolution on the ability of the model to represent a cold air outbreak? iii) Are model physics or dynamical formulations more important for the fidelity of the simulation? iv) Are convective parametrizations required for km-scale simulations?

2 Description of case

The case is from 31st January 2010 and has been described in Field et al. (2014). It is a cold air outbreak located between Iceland, Norway and Scotland. It is characterised by a polar low feature at 64^{o}N, 4^{o}W to the West of Norway, and a high pressure ridge stretching between the Azores and Iceland (fig. 7a). There is a strong northerly flow between Iceland and Norway, stretching from north of 70^{o}N to south of 60^{o}N over England. This synoptic situation follows the climatological pattern identified for cold air outbreaks in the Greenland-Iceland-Norwegian sea areas by Kolstad et al. (2009).

The flow brings cold air from the Arctic sea ice over the warmer (5-10^{o}C) seas to the south. Parcels traverse $\sim$700km in 12 hours (~ 15 m s^{-1}). North west of the Faroe Islands the boundary layer is $\sim$1km deep and characterised by a stratocumulus cloud deck with close to complete cloud cover. Droplet concentrations from satellite based estimates are 50-100 cm^{-3}. Even though the stratocumulus region is over colder sea temperatures than the convective region there is likely to be little ice, but there were no insitu observations to confirm this. The reason for this dearth of ice in the stratocumulus region relative to the convective region is potentially linked to the warmer cloud top temperatures and hence reduced heterogeneous nucleation rates than for the deeper colder topped convective cloud. Liquid water paths reached ~ 0.3 kg m^{-2} based on remote sensing estimates. Eventually, as the air moves over warmer sea, the boundary layer begins to grow and the stratocumulus cloud gives way to cumulus that reaches up to $\sim$3km (red box in fig 7b). Aircraft measurements indicate that in

the cumulus region the ice concentrations (maximum size, $D > 100\,\mu$m) reach $\sim$ 10 L^{-1} and droplet concentrations ~ 10 cm^{-3} with ice and liquid water contents of ~ 0.3 g m^{-3} and $\sim$ 0.1 g m^{-3}, respectively. Aircraft based estimates of integrated water paths for the cumulus region are 0.06 ± 0.03 kg m^{-2} for liquid and in the range of 0.08-0.20 kg m^{-2} for ice. A schematic of the evolution of the boundary layer and cloud is shown in fig 7c.

3 Models

Output from nine different models (UM: Unified Model, WRF: Weather Research and Forecasting model (2 configurations), NHM: non-hydrostatic model, "ASUCA", Meso-NH: mesoscale non-hydrostatic, AROME: Applications of Research to Operations at MesoscalE, ALADIN: Aire Limitée Adaptation dynamique Dévelopment INternational, EC: Environment Canada) was submitted for the comparison. Table 1 summarises the models and the choices for microphysics, boundary layer, convection and advection. The models were run with grid spacings of 16, 8, 4, 2, 1km grid spacing (AROME only 4,2,1) over a domain 1600km (north-south) x 800 km (east-west). Sets of simulations were carried out with convection parametrization on (convection-on) and with convection parametrization off (convection-off).

Apart from AROME and ALADIN that used ARPEGE analysis, the models were run for 24 hours from ECMWF analysis (12 Z 30th January 2010), with the bulk of the analysis carried out at around 12Z 31st January. Some models used a parent global model to provide boundary conditions to drive the inner nested model used to provide the data for the intercomparison. Other models used 6 hourly ECMWF analyses to provide boundary conditions for a large area regional model that in turn provided boundary conditions for the inner nest used in the intercomparison.

Tests were carried out with the UM to assess the impact of using a different starting analysis and vertical level set. For the sensitivities a UM analysis was used instead of the ECMWF analysis and for the vertical level sensitivity test the level spacings were halved to increase the number of levels from 70 to 140. The results indicate that while the changes are systematic they are the same size as the variability represented in the control run.

tableDescription of models used.

Model	contributor	main ref	microphysics	boundary layer	convection off	convection on	advection	other remarks	levels(1km/total/tm)

Unified Model	Met Office	Walters et al.2017 GA6(global)OS 37(regional)	Wilson and Ballard 1999	Non-local boundary layer scheme (Lock et al. 2000)	no convection	global model settings for deep shallow and mid conv (Walters et al.2017)	Semi-Lagrangian (Wood et al. 2015)	Uses the 'Smith cloud scheme' to represent subgrid distribution of humidity. It assumes a triangular distribution of humidity with a predefined width (called RHcrit). When the grid box 's=total water mixing ratio/saturated mixing ratio' is RHcrit (0.8) cloud can start to form. With increasing water the cloud fraction in the grid box	16/29/70 m

								increases eventually reaching 1.0.	
WRF	NCAR		Thompson microphysics	YSU PBL,		Tiedtke cumulus option	ARW dynamical core. Nonhydrostatic, compressible, time-splitting with semi-implicit sound waves, 3rd order Runge-Kutta time steps, C-grid staggering, 5th order horizontal and 3rd order vertical advection,terrain-following mass-based		7/ 5/29km

							vertical coordinate.		
WRF	NOAA	Benjamin et al. (2016), Skamarock et al. (2008)	Thompson DM incl graupel and hail	Mellor-Yamada-Nakanishi-Niino (MYNN) scheme, with mods to use a non-local BouLac scheme in the free atmosphere and a surface layer length scale that varies with surface stability parameter.		Grell-Freitas scheme. Scale-aware scheme, transforms into a shallow-Cu scheme at high-resolution (< 5 km), and is shut off entirely at grid spacings below 1 km. This is run at every time-step.	Same as NCAR, but 5th order vertical advection instead of 3rd order		17 62/27km
NHM	JMA	Saito et al. 2006 and Saito et al. 2007	physics implenented through	The improved Mellor-Yamada-Nakanishi-Nii		Kain-Fritsch (KF) scheme	finite difference method employing the		11 58/20km

			"Physics Library" (Hara et al. 2012). 6-class single moment cloud microphysics based on Lin (1983).	no (MYNN) scheme (Nakanishi and Niino 2009)			leap-frog time integration method, forth-order difference method with an artificial advection correction scheme and linear and non-linear numerical diffusions.		
ASUCA	JMA	Ishida et al. 2009, 2010	physics implemented through "Physics Library" (Hara et al. 2012). 6-class single moment cloud microphysics based on Lin	The improved Mellor-Yamada-Nakanishi-Niino (MYNN) scheme (Nakanishi and Niino 2009)		Kain-Fritsch (KF) scheme. Uses different triggering at 2 and 1km resolution	finite volume method with the 3rd order Runge-Kutta time integration and upwind 3rd order advection scheme with a	All of the fields are the sum of the resolved and subgrid. Method 1 forcing driven by dx=20km global	11 58/20km

			(1983).				flux limiter and without numerical diffusions.		
Meso-NH	CNRM-Meteo-France	Lafore et al., 1998	Mixed-phase one-moment microphysical scheme						
(Pinty and Jabouille 1998) with two liquid and 3 ice categories	A prognostic turbulent kinetic								
energy scheme (1.5 order, Cuxart et al., 2000) in 1D mode with the Bougeault-Lacarrere (1989)									
mixing length	No deep or shallow convection	Deep convection scheme is the mass flux							
scheme of Bechtold et al. (2001) at 16km, 8km and									

4km. The shallow convection is an EDMF			
scheme (Pergaud et al., 2009) at all resolutions.	Eulerian with the 5th-order WENO advection		
scheme for the wind, associated to a 3th order RK temporal scheme, and the PPM (Colella and			
Woodward, 1984) advection scheme for other variables.	Method 2, using ECMWF analyses		
every 6h to generate LBCs, 45 vertical levels	14/24/45/19km		
AROME	CNRM-Meteo-France	Seity et al., 2011	Mixed-phase one-moment microphysical

			scheme	
(Pinty and Jabouille 1998) with two liquid and 3 ice categories	A prognostic turbulent kinetic			
energy scheme (1.5 order, Cuxart et al., 2000) in 1D mode with the Bougeault-Lacarrere (1989)				
mixing length	No deep or shallow convection	Only shallow convection from an EDMF		
scheme (Pergaud et al., 2009) at 4km, 2km and 1km	Spectral, semi-implicit semi-Lagrangian			
Arpege initial and boundary conditions	15/26/60/51km			
Aladin	CHMI	Termonia et al. 2017	ALARO-0	Pseudo-prognostic version.

			Clouds - a scheme based on the Xu-Randall approach (Xu, K. M. and D.A. Randall, 1996 . The microphysics is a one moment Kessler type, it is not published as a whole but there is an original treatment of the sedimentation problem (Geleyn et al. 2008).	TKE scheme (Geleyn et al. 2006). Horizontal diffusion: Semi-Lagrangian based grid-point local diffusion (Váňa et al. 2008)	
		Moist deep convection : the 3MT	spectral in horizontal, finite	Flux-conservative thermodynami	15/27/60/50km

		(Modular Multi-scale Microphysics and Transport) scheme, specifically developed for the grey zone of convection (Gerard et al. 2009). This scheme was switched on or off as the only difference between the two sets of experiments. It is important to note that we use the same microphysics in both cases (3MT on or off), in the case the 3MT	differences in vertical; Time scheme and advection: Two-time-level Semi-Implicit Semi-Lagrangian. Bénard et al. 2010	c equations in a mass-weighted framework	

		is active we treat both the resolved and sub-grid condensations.							
EC	Environment Canada	Gerard et al. 2014	Two-moment bulk microphysics (Milbrandt and Yau 2005a,b) with two liquid categories and four ice categories	A prognostic turbulent kinetic energy scheme (1.5 order, Belair 1999)	No deep or shallow convection, but PBL clouds are still active	Kain-Fritsch (1990) scheme for deep convection and a Kuo-type closure for shallow convectin (Belair, 2005). Trigger for deep convection adjusted for the operational system with 2.5 km grid spacing.	Gridpoint based two time-level implicit semi-lagrangian.		

Four of the models use semi-Lagrangian advection (AROME, CHMI,EC, UM). For convection, two models use 'global settings' that are almost unchanged for all of the convection-on simulations (WRF-NCAR, UM). Four models have some scale-aware convection treatment (WRF-NOAA, Meso-NH, NHM and ASUCA) either through an approach that gradually shuts off convection as resolution increases (WRF-NOAA) or by not doing deep convection for the higher resolution simulations (Meso-NH) or by using different convective triggering thresholds at the highest resolutions (NHM, ASUCA).

Interestingly there are a few pairs of models that either share the same physics or dynamical cores. AROME and Meso-NH have the same physics but different dynamical cores and use different initialisations (ARPEGE, ECMWF). Similarly, NHM and ASUCA also have the same physics but different dynamical cores. While two pairs of models (NOAA and NCAR, AROME and ALADIN) share a dynamical core but different microphysics, boundary layer and convection.

4 Results

4.1 General comparison

Outgoing longwave flux at the top of the atmosphere from each model for the 1km, 16km and convection-on and convection-off simulations are shown for T+24 hours into the simulation (Figures 7,7,7).The darker shades represent greater fluxes from warmer surfaces such as the sea surface or clouds lower down in the troposphere. These figures can be compared qualitatively with the image shown in fig 7b. Comparison of the 1km convection-off panels shows that the polar low feature is consistently reproduced in size and location by all of the models. In the southern half of the domain, all of the models show convective clouds. To the northwest of the domain most models show the encroaching cirrus from an extratropical cyclone to the west of the study region. In the northern portion of the domain the models show different low cloud morphologies ranging from cloud streets to more closely packed convection. The 16km simulations with convection-off again show the polar low to be of similar size and location between models, but there is generally more widespread low cloud. For the convection-on simulations at different resolutions the results are more varied. This is due in part to different models having varying levels of model resolution awareness built into their convection parametrizations. For the 1km convection-on results, some models essentially switch off parametrized convection and

look the same as the convection-off simulation (ASUCA, AROME, CHMI, EC, NOAA), while others experience a strong impact from the parametrized convection (Meso-NH, UM, NCAR, NHM).

For more a quantitative comparison, two regions have been focused on: a stratocumulus region in the north (blue box in fig 7b) and a convective region in the south (red box in fig 7b). For each model, mean values and variances are calculated in 100km regions for the different resolutions and for the case where convection is on or off. These results are then compared with aircraft and satellite observations (Liquid Water Path from the Advanced Microwave Scanning Radiometer, Wentz 1998, and broadband fluxes from the Clouds and the Earth's Radiant Energy System , Wielicki et al. (1996), see Field et al. 2014 for more details) around 12Z 31st January 2010.

4.2 Stratocumulus

In this region the satellite observations in fig. 7b indicate widespread closed cell layer cloud with almost complete cloud cover. It is clear that most of the 1-km models are not able to reproduce this behaviour and instead tend towards open cellular shallow convection.

Mean outgoing broadband fluxes over a 100km x 100km region in the stratocumulus dominated part of the domain for convection-off simulations are shown in figure 7 for short- and longwave. For each model the results for the different model resolutions are given. Results from the convection-off simulations differ from the satellite observed value and show that the simulated fluxes for both long and shortwave deviate more from the observations with increasing resolution.There is more model-to-model variability at 1km than there is at 16km for the SW fluxes. With the convection-on (fig.7) some models show monotonic changes with increasing resolution, but there is generally less variation across the models and with changing resolution when compared to the convection-off simulations. For some models (CHMI, NCAR, Meso-NH) the convection-on simulations agree better with the observations at 1km than the convection-off simulations suggesting that the parametrization at these resolutions may still be beneficial. Overall, the simulations have 10-30 W m^{-2} (5-15%) too much outgoing longwave flux and underestimate the outgoing shortwave flux by 20-100 W m^{-2} (10-60%) suggesting insufficient cloud cover.

Liquid water path for the convection-off simulations (fig.7) shows a very wide range that tends to decrease with increasing

resolution but also drifts from the observed value. Only two simulations (EC, NOAA) have a value consistent (> 0.1 g m^{-3}) with the observations for some resolutions. For convection-on the liquid water path is lower than for convection-off (fig.7) and both are generally much lower than the estimate derived from passive microwave observations (Field et al. 2014). There are no observational estimates of IWP for the stratocumulus region. Nevertheless, it can be seen (fig.7b) that the models estimates span an order of magnitude from 0.01 to 0.1 kg m^{-2} with no obvious trend with resolution.

Profiles of potential temperature and total water (fig 7) show that there is less model spread in the 1km simulations when compared to the 16km simulations. For an individual model the difference between convection on and off is less than the spread between models. Generally, the boundary layer is deeper, warmer and drier for the convection-on simulations relative to the convection-off simulations. This is consistent with parametrized convection more efficiently mixing the boundary layer than when it is done by explicit convection. The profiles look well-mixed in the bottom kilometre of the profile. The top of the boundary layer varies between models over a few hundred meters.

Field et al. (2014) demonstrated that modifying the boundary layer scheme to promote a mixed-layer character in the dynamical conditions experienced in the stratocumulus region leads to improved cloud cover and radiative fluxes. Those changes were not introduced to the operational UM due to the proximity of the northern boundary to the British Isles and have not been included in these results that make use of an operational configuration.

4.3 Cumulus

Concentrating on a convective region to the south, both the convection-off and convection-on simulations show a convergence towards the observed long and shortwave flux values with increased resolution , but with a broader range of simulated longwave broadband fluxes with convection-on (fig 7). Generally, for the convective region there is better agreement between the models and the observations of broadband flux than was seen for the stratocumulus region.

For the convection-off simulations the liquid water path tends to decrease with increased resolution for most of the models (fig 7). About a third of the models have liquid water path values within the range of the observations at the highest model resolution. The rest of the models have lower values (factor of 2-5). The range of LWP spans an order of magnitude and this range across the models is larger than the change seen by each model as a function of resolution. Some of the models which present an

underestimation of LWP are in better agreement with the aircraft measurements of IWP, and only one (ASUCA) presents correct values for both fields. At 1 km resolution, the intermodel spread is high for IWP. Three of the simulations produce good agreement with the observations (based on integrating the aircraft measurements) (NCAR, Meso-NH and ASUCA) and a slight monotonic decrease in IWP with increasing resolution. The other models exhibit lower IWP. For convection-on (fig 7), the results are more variable, but the liquid water path values are consistently low with only one model (ASUCA) producing similar values to the observations at the 1km resolution while two other models have better agreement at the coarsest resolution (EC and NOAA). The intermodel spread for IWP is reduced with convection-on at 1 km.

Profiles of potential temperature and total water (fig 7) indicate reduced model spread for the 1km simulations compared to the 16km simulations. The simulations generally agree with the aicraft observations although the potential temperature in the lowest kilometre tends to be colder for most of the models than suggested by the observations. For a given model the difference between convection on and convection off simulations is less than inter-model differences. Liquid and ice water content profiles (fig. 7) for the 1km simulation (16km simulations exhibit more spread) show a peak in liquid water at heights ranging from 1 to 2.5km. The aircraft observations suggest that the liquid water contents are greatest between 2 and 2.5km. Some models produce liquid water contents of the same magnitude (0.03g/kg) as the aircraft observations, but most do not. The modelled ice water contents are generally smaller than the peak observed ice water contents (0.15g/kg). Some of the convection-on models (Meso-NH, AROME) produce deeper ice water profiles that are closer to the observations than any of the convection-off simulations at 1km. For the liquid profiles, convection-on generally produces less liquid.

Taking a larger region (yellow box in fig1b) three snapshots of 10 min rain accumulations at 11,12,13 UTC were combined to provide precipitation statistics from each of the models (fig. 7) around the same time as the comparison with observations has been made. Domain averaged 10 minute rain accumulations across all resolutions for all models with convection-off lies within ± 0.09 mm of the multimodel mean of ~ 0.09 mm and for 1km, the models lie within ± 0.07mm of 0.09 mm. Three models exhibit approximately constant accumulations of rain with changing resolution (CHMI, NCAR, UM). Most models show a generally increasing monotonic change with increasing resolution, but two models exhibit a distinct peak in rain accumulation at 4km resolution (NHM, AROME). Results from an earlier version of the UM exhibited a peak in rainrate at intermediate resolutions, but the results presented here used enforced moisture conservation for semi-lagrangian advection (Aranami et al. 2014) that have reduced this tendency. The results from the convection-off simulations exhibit similar values to the convection-on counterpart, but generally

present less or little variation with resolution.

Rain accumulations can be explored further by examining histograms. All of the rainrate histograms follow the usual gamma distribution with lower frequency at larger accumulations. As may have been expected, the models that display little change in their domain mean accumulated rain with resolution also do not exhibit much difference in the rain accumulation histograms for the different resolutions. That is not the case for the models that exhibit a peak in the rain accumulation at an intermediate resolution. These exhibit an increased frequency of greater rainrates at these intermediate resolutions (not shown).

5 Discussion

Comparing the pairs of models that have the same physics but different dynamical core first, it can be seen by looking at the 1km convection-off LW panels in figs 7,7,7 that differences in the dynamical core can lead to large differences in the cloud morphology. Fig 7e and fig. 7i show well developed cloud streets in one simulation (NHM) while the other (ASUCA) has more homogeneous cloud in the stratocumulus region. For the stratocumulus region this more homogenous cloud for ASUCA translated into improved LWP and radiation comparisons with observations at 1km model grid spacing. For the cumulus region both models have isolated cumulus clouds but ASUCA has improved LWP, IWP and shortwave radiation when compared to observations. In both the cumulus and stratocumulus region, the NHM model has a slightly deeper boundary layer than the ASUCA model.

For the AROME-Meso-NH pair at 1km one of the models (Meso-NH, fig 7e) has small but densely spaced cumulus clouds in the stratocumulus region. The other (AROME, fig 7i) has more layer cloud but it is quite broken and eventually begins to form into wave clouds before breaking up into cumulus further downstream. In terms of comparison to the observations, the Meso-NH model produces better agreement in condensed water, but not area averaged radiation. In the cumulus region, the AROME convective elements appears larger than the Meso-NH convective elements, but the Meso-NH has greater condensed water paths. Both underestimate the LWP but more accurately reproduce the IWP. These small differences are likely related to the different dynamical formulation adopted in these models and/or the different sources used for initialisation and boundary condition of the models (ARPEGE and ECMWF). The main difference between the models at 1km is that the shallow convection scheme 'switches off' at 1 km grid spacing for AROME leading to identical convection-on/off results, while differences are significant between convection-on and convection-off for Meso-NH, with better agreement to observations for convection-on (shallow convection only activated).

Turning now to the pair of models with the same dynamical core but different physics: NOAA (fig 7e) and NCAR (fig 7i) both exhibit convective elements in the stratocumulus and convective region. The NCAR convection appears to increase in size more rapidly than the NOAA convective elements. NOAA LWP and LW are improved in the stratocumulus region, but the LWP and LW are similar in the convective region with the NCAR model exhibiting improved IWP compared to observations. Sensitivity to the activation of the convection scheme is dramatically different between these two models with the NCAR model developing more widespread cloud.

In terms of rainrates at 1km grid spacing in the larger convective region used for fig. 7 it is difficult to conclude whether the pair of models with different physics but the same dynamical core has a larger difference than the pairs of models with the same physics but different dynamical cores. Thus it appears for this case, at 1km grid spacing and convection-off, that the dynamical core, microphysics and turbulence can play an important role in controlling the morphology of clouds.

Decreases in model spread in terms of the thermodynamic profile and broadband fluxes with decreasing grid spacing as indicated in figs 9,10 and 13 suggest that for the convection-off simulations, the improved representation of the dynamics is having a positive effect on the quality of the simulations. However, for many metrics e.g. LWP and IWP, no convergence between the models is seen with resolution.

For the models in this study the differences in rain accumulation with resolution are quite large and in general have not converged even at 1 km grid spacing. Moreover, changes in resolution appear to make more difference than variations in model physics when the dynamical core is the same (e.g. NCAR, NOAA) or changes in the dynamics when the physical parametrizations are the same (NHM, ASUCA). It seems sensible then to attempt to understand how the interplay between physics and dynamics, the scale of the phenomenon and the resolution of the model combine to control predictions such as accumulated rain.

The effective resolution is the actual finest well-resolved scale of a model. For a given grid spacing, a model will produce resolved structures depending not only on the grid spacing but also on the diffusion (implicit and explicit) of the model. The difference between the models may come from the numerical schemes (implicit diffusion), but also on the subgrid transport schemes (explicit diffusion). For instance, due to its efficient but diffusive numerical schemes, AROME's effective resolution is larger than that of Meso-NH (Ricard et al. 2013). Subgrid transport schemes are the turbulence and convection parametrizations that both limit the variability of the resolved fields. The vertical velocity field is a resolved field representative of the effective resolution of a model. For instance, it is clear in Fig.2-4 that UM or NCAR present finer structures with convection-off and coarser structures with

convection-on, as their convection scheme probably produces strong subgrid updrafts. Vertical velocity is also representative of the partition resolved/subgrid motions. The standard deviation of the vertical velocity field is larger at finer resolutions as more of the flow is explicitly resolved but for this comparison across scales we have regridded onto a common 16km grid scale.

The standard deviation of the resolved vertical velocity that has been area-averaged and regridded onto the 16km resolution grid as a function of altitude and resolution is shown in fig. 7 and 7. It is clear that the standard deviation of the vertical velocity is generally higher in the convective region than the stratocumulus region as might be expected. There is a tendency for the vertical velocity standard deviation to be less when the convection parametrization is on than when it is off. Again this might be expected due to the convection parametrization removing instability from the atmosphere. For the convective region and the convection-on simulations the UM, NHM, Meso-NH and CHMI show that the standard deviation increases with increasing resolution, while NCAR, NOAA and ASUCA tend to display a non monotonic behaviour with the standard deviation of the vertical velocity increasing at intermediate resolutions. AROME presents the largest values of vertical velocity standard deviation. Differences are less clear for the stratocumulus region where contributions from other dynamical effects such as gravity waves and the details of the boundary layer parametrization will be important.

The simulations mainly fall outside of the grey zone for the stratocumulus region, exhibit a lack of intermodel consistency and poor comparison with the observations. It has been shown in previous analysis of this case (Field et al. 2014) that forcing the boundary layer representation to diagnose a well-mixed layer for this region was successful in generating stratiform cloud cover there. In order for the simulations in this region and at these resolutions to capture the behaviour of the cloud and boundary layer structure in this regime needs to be captured better by the boundary layer parametrization. In contrast, it can be argued that for the convective region the models are beginning to probe the grey zone in the highest resolution simulations. For these simulations there is evidence that the models begin to compare better with the observations and converge as evidenced by the reduction in inter-model spread (e.g. figs 7, 7) but without necessarily reaching convergence.

6 Conclusions

A model intercomparison of a cold air outbreak case study has been performed. The models used included several operational Numerical Weather Prediction systems. Simulations were carried out at a range of grid spacings from 16 to 1km with

convection parametrizations on or off and compared to observations at 24 hours into the simulation. All of the models and resolutions capture the large scale structure of the event with a strong northerly cold outflow and a consistent size and location for the polar low feature.

There was more consistency between models for convection-off simulations compared to convection-on simulations. This is partly attributed to the differing character of the convective simulations: some are scale aware while others use constant settings appropriate for global model resolutions. However, scale-aware parametrizations can still lead to different precipitation versus model resolution behaviour.

All models struggled with representing the stratocumulus region of cold air outbreak. There was a lack of model consistency and models tended towards carrying out explicit convection at the highest resolution. This resulted in a tendency for models to generate open cellular structures, a lack of cloud cover and reduced condensed water amounts when compared to the observations.

In the convective region,the cloud morphology in all simulations tended towards open cellular convection. For this region, the models showed some convergence for the convection-off simulations and reasonable agreement with the observations in terms of broadband fluxes. For the condensed liquid water path the model estimates spanned an order of magnitude but individual models varied much less than this as a function of grid spacing. In addition to generally suffering from this low bias in total condensate mass, only a few of the models were capable of generating sufficient cloud ice at the top of the boundary layer to match the observations.

Comparing pairs of models that share the same physics or dynamical core indicates that both of these model components have strong influences on the morphology, the microphysical and radiative characteristics of the clouds.

The simulations do not really probe the grey zone for the stratocumulus region. Finer grid spacings ($\sim$ 100 m) are required. For km-scale models a realistic representation of these clouds most likely requires a parametrized approach, such as in the treatment of the boundary layer, to compensate for the models inability to resolve the motions at km-scale and to nudge the models to a more well-mixed boundary layer solution more appropriate for these clouds. There is greater inter-model agreement and improved comparison with observations for the convective region for some metrics such as broadband fluxes and the thermodynamic structure of the boundary layer. This may be because the grey zone is being probed more successfully by the higher resolution simulations.

7 References

Aranami, K., T. Davies, et al. (2015). "A mass restoration scheme for limited-area models with semi-Lagrangian advection." Quarterly Journal of the Royal Meteorological Society 141(690): 1795-1803.

Bechtold P., Fravalo C. and J-P Pinty, 1992: A study of a two-dimensional cloudiness transition during a cold air outbreak event. Boundary-Layer Met., 60, 243-270.

Bechtold, P., E. Bazile, F. Guichard, P. Mascart and E. Richard, 2001: A mass flux convection scheme for regional and global models. Quart. J. Roy. Meteor. Soc., 127, 869-886.

Bélair S., Mailhot J., Claude Girard, and Paul Vaillancourt, 2005: Boundary Layer and Shallow Cumulus Clouds in a Medium-Range Forecast of a Large-Scale Weather System. Mon. Wea. Rev., 133, 1938-1960.

Bélair S., Mailhot J., J. Walter Strapp, and J. Ian MacPherson, 1999: An Examination of Local versus Nonlocal Aspects of a TKE-Based Boundary Layer Scheme in Clear Convective Conditions. J. Appl. Meteor., 38, 1499-1518.

Belair, S., J. Mailhot, et al. (2005). "Boundary layer and shallow cumulus clouds in a medium-range forecast of a large-scale weather system." Monthly Weather Review 133(7): 1938-1960.

Bénard, P., Vivoda, J., Mašek, J., Smolíkoá, P., Yessad, K., Smith, C., Brožková, R., and Geleyn, J.-F.: Dynamical kernel of the Aladin-NH spectral limited-area model: Revised formulation and sensitivity experiments., Quart. J. Roy. Meteor. Soc., 136, 155?169, 2010.

Benjamin, Stanley G., Stephen S. Weygandt, John M. Brown, Ming Hu, C. R. Alexander, T. G. Smirnova, J. B. Olson, E. P. James, D. C. Dowell, G. A. Grell, H. Lin, S. E. Peckham, T. L. Smith, W. R. Moninger, J. S. Kenyon, G. Manakin. A North American Hourly Assimilation and Model Forecast Cycle: The Rapid Refresh. Mon. Wea. Rev., 2016 144:4, 1669-1694, DOI: http://dx.doi.org/10.1175/MWR-D-15-0242.1

Bodas-Salcedo, A., et al., 2014: Origins of the Solar Radiation Biases over the Southern Ocean in CFMIP2 Models. J. Clim. doi: 10.1175/JCLI-D-13-00169.1

Bougeault P. and P. Lacarrère, 1989: Parameterization of orography-induced turbulence in a mesobeta-scale model. Mon. Wea. Rev., 117, 1872-1890

Brousseau, P., Seity, Y., Ricard, D. and Léger, J. (2016), Improvement of the forecast of convective activity from the AROME-France system. Q.J.R. Meteorol. Soc., 142: 2231-2243. doi:10.1002/qj.2822

Bryan, G. H., J. C. Wyngaard, et al. (2003). "Resolution requirements for the simulation of deep moist convection." Monthly Weather Review 131(10): 2394-2416.

Chaboureau J.-P., and P. Bechtold, 2002: A simple cloud parameterization derived from cloud resolving model data: Diagnostic and prognostic applications. J. Atmos. Sci., 59, 2362- 2372.

Clark P.A, Roberts N.M., Lean H.W., Ballard S.P., Charlton-Perez C., 2016: Convection Permitting Models: A Step Change in Rainfall Forecasting. Met Apps 23 165-181.

Collela P, Woodward PR. 1984. The piecewise parabolic method (PPM) for gas dynamical simulations. J. Comput. Phys. 54: 174-201.

Cuxart J., P. Bougeault J.-L. Redelsperger, 2000: A turbulence scheme allowing for mesoscale and large-eddy simulations. Quart. J. Roy. Meteor. Soc., 126, 1-30

Field, P. R., R. J. Cotton, et al. (2014). "Improving a convection-permitting model simulation of a cold air outbreak." Quarterly Journal of the Royal Meteorological Society 140(678): 124-138.

Gal-Chen T, Somerville RCJ. 1975. On the use of a coordinate transformation for the solution of the NavierStokes equations. J. Comput. Phys. 17: 209-228, doi:10.1016/0021-9991(75)90037-6.

Gao, Y., L. R. Leung, et al. (2017). "Sensitivity of US summer precipitation to model resolution and convective parameterizations across gray zone resolutions." Journal of Geophysical Research-Atmospheres 122(5): 2714-2733.

Geleyn, F. Vana, J. Cedilnik, M. Tudor, B. Catry, 2006: An intermediate solution between diagnostic exchange coefficients and prognostic TKE methods for vertical turbulent transport, WGNE Blue Book

Geleyn, J.-F., B. Catry, Y. Bouteloup and R. Brožková, 2008: A statistical approach for sedimentation inside a micro-physical precipitation scheme , Tellus A, Volume 60 Issue 4, pp 649-662

Gerard, L., Piriou, J.-M., Brožková, R., Geleyn, J.-F., and Banciu, D.: Cloud and precipitation parameterization in a meso-gamma scale operational weather prediction model, Mon.Wea. Rev., pp. 3960?3977, 2009.

Girard C., Plante A.,Desgagné M.,McTaggart-Cowan R., Côté J., Charron M., Gravel S.,Lee V., Patoine A., Qaddouri A., Roch M., Spacek L., Tanguay M., Vaillancourt P.A., and Zadra A., 2014: Staggered Vertical Discretization of the Canadian Environmental Multiscale (GEM) Model Using a Coordinate of the Log-Hydrostatic-Pressure Type. Mon. Wea. Rev., 142, 1183-1196.

Hara, T., K. Kawano, K. Aranami, Y. Kitamura, M.Sakamoto, H. Kusabiraki, C. Muroi, and J. Ishida, 2012: Development of the

Physics Library and its application to ASUCA. CAS/JSC WGNE Res. Activ. Atmos. Oceanic Modell., 42, 5.05-5.07

Holloway, C. E., S. J. Woolnough, et al. (2012). "Precipitation distributions for explicit versus parametrized convection in a large-domain high-resolution tropical case study." Quarterly Journal of the Royal Meteorological Society 138(668): 1692-1708.

Honnert, R., V. Masson, F. Couvreux : A Diagnostic for Evaluating the Representation of Turbulence in Atmospheric Models at the Kilometric Scale, Journal of the Atmospheric Sciences, 2011, 68, 12, 3112

Hwang, Y-T., D.M.W. Frierson, 2013: Link between the double-Intertropical Convergence Zone problem and cloud biases over the Southern Ocean, PNAS, doi:10.1073/pnas.1213302110

Ishida, J., C. Muroi, and Y. Aikawa, 2009: Development of a new dynamical core for the nonhydrostatic model. CAS/JSC WGNE Res. Activ. Atmos. Oceanic Modell., 39, 0509-0510.

Ishida, J., C. Muroi, K. Kawano, and Y. Kitamura, 2010: Development of a new nonhydrostatic model ASUCA at JMA. CAS/JSC WGNE Res. Activ. Atmos. Oceanic Modell., 40, 0511-0512

Kain J. S. and J. M. Fritsch (1990) : A One-Dimensional Entraining/Detraining Plume Model and Its Application in Convective Parameterization, J. Atmos. Sci., 47, 2784-2802

Kain J.S. and Fritsch J.M., 1990: A One-Dimensional Entraining/Detraining Plume Model and Its Application in Convective Parameterization. J. Atmos. Sci., 47, 2784-2802.

Kolstad EW, Bracegirdle TJ, Seierstad IA. 2009. Marine cold-air outbreaks in the North Atlantic: Temporal distribution and associations with large-scale atmospheric circulation.Clim. Dyn.33:187 ? 197.

Korolev, A. V., Isaac, G. A., Cober, S. G., Strapp, J. W. and Hallett, J. (2003), Microphysical characterization of mixed-phase clouds. Q.J.R. Meteorol. Soc., 129: 39-65. doi: 10.1256/qj.01.204

Lafore J., and Coauthors, 1998: The Méso-NH atmospheric simulation system. Part I: Adiabatic formulation and control simulation. Ann. Geophys., 16, 90-109.

Lin, Y. , R. D. Farley, H. D. Orville (1983) : Bulk Parameterization of the Snow Field in a Cloud Model, J. Appl. Meteor, 22, 1065-1092

Lock, A. P., A. R. Brown, et al. (2000). "A new boundary layer mixing scheme. Part I: Scheme description and single-column model tests." Monthly Weather Review 128(9): 3187-3199.

J. Mailhot, S. Bélair, M. Charron, C. Doyle, P. Joe, M. Abrahamowicz, N. B. Bernier, B. Denis, A. Erfani, R. Frenette, A. Giguère,

G. A. Isaac, N. McLennan, R. McTaggart-Cowan, J. Milbrandt, and L. Tong, 2010: Environment Canada's Experimental Numerical Weather Prediction Systems for the Vancouver 2010 Winter Olympic and Paralympic Games. Bull. Amer. Meteor. Soc., 91, 1073-1085.

Milbrandt, J. A. and M.K. Yau. 2005. A multimoment bulk microphysics parameterization. Part I: Analysis of the role of the spectral shape parameter. J. Atmos. Sci. 62:3051-3064.

Milbrandt, J. A. and M.K. Yau. 2005. A multimoment bulk microphysics parameterization. Part II: A proposed three-moment closure and scheme description. J. Atmos. Sci. 62:3065-3081.

Moore, G. W. K. (2013), A climatology of vessel icing for the subpolar North Atlantic Ocean. Int. J. Climatol., 33: 2495-2507. doi:10.1002/joc.3604

Nakanishi M. and H. Niino (2009) : Development of an Improved Turbulence Closure Model for the Atmospheric Boundary Layer, J. Meteor. Soc. Japan, 87, 895-912

Pearson, K. J., G. M. S. Lister, et al. (2014). "Modelling the diurnal cycle of tropical convection across the 'grey zone'." Quarterly Journal of the Royal Meteorological Society 140(679): 491-499.

Pergaud J., V. Masson, S. Malardel and F. Couvreux, 2009: A parameterization of dry thermals and shallow cumuli for mesoscale numerical weather prediction. Bound.-Layer Meteor., 132, 83-106.

Pinty, J.-P. and Jabouille , P. 1998. A mixed-phase cloud parame terization for use in amesoscale non hydrostatic model: Simulations of a squall line and of orographic precipitation. Pp. 217-220 in Proceedings of Conference on Cloud Physics, 17-21 August 1998, Everett,USA

Redelsperger, J.-L., and G. Sommeria, 1986: Three-dimensional simulation of a convective storm: Sensitivity studies on sub-grid parameterization and spatial resolution. J. Atmos. Sci., 43, 2619 -2635

Ricard, D., C. Lac, S. Riette, R. Legrand, and A. Mary, Kinetic energy spectra characteristics of two convection-permitting limited-area models AROME and Meso-NH, Quart. J. Roy. Meteor. Soc.,139, 1327-1341, 2013.

Saito, K, T. Fujita, Y. Yamada, J. Ishida, Y. Kumagai, K. Aranami, S. Ohmori, R. Nagasawa, S. Kumagai, C. Muroi, T. Kato, H. Eito and Y. Yamazaki (2006) : The Operational JMA Nonhydrostatic Mesoscale Model, Mon. Wea. Rev, 134, 1266-1298

Saito, K. , J. Ishida, K. Aranami, T. Hara, T. Segawa, M. Narita and Y. Honda (2007) : Nonhydrostatic Atmospheric Models and Operational Development at JMA, J. Meteor. Soc. Japan, 85B, 271-304

Sakradzija, M., A. Seifert, et al. (2016). "A stochastic scale-aware parameterization of shallow cumulus convection across the convective gray zone." Journal of Advances in Modeling Earth Systems 8(2): 786-812.

Schultz D.M., Arndt D.S., Stensrud D.J., and Hanna J.W., 2004: Snowbands during the Cold-Air Outbreak of 23 January 2003. Mon. Wea. Rev., 132, 827-842.

Y. Seity, P. Brousseau, S. Malardel, G. Hello, P. Bénard, F. Bouttier, C. Lac, and V. Masson, 2011: The AROME-France Convective-Scale Operational Model. Mon. Wea. Rev., 139, 976-991. doi:http://dx.doi.org/10.1175/2010MWR3425.1

Simmons, A., and D. M. Burridge, 1981: An energy and angular-momentum conserving finite difference scheme and hybrid vertical coordinates. Mon. Wea. Rev., 109, 758-766.

Skamarock, W. C., J. B. Klemp, J. Dudhia, D. O. Gill, D. M. Barker, M. G. Duda, X.-Y. Huang, W. Wang, and J. G. Powers, 2008: A description of the Advanced Research WRF Version 3. NCAR Tech Notes-475+STR

Smith, R. N. B. (1990). "A SCHEME FOR PREDICTING LAYER CLOUDS AND THEIR WATER-CONTENT IN A GENERAL-CIRCULATION MODEL." Quarterly Journal of the Royal Meteorological Society 116(492): 435-460.

Stein, T. H. M., D. J. Parker, et al. (2015). "The representation of the West African monsoon vertical cloud structure in the Met Office Unified Model: an evaluation with CloudSat." Quarterly Journal of the Royal Meteorological Society 141(693): 3312-3324.

Piet Termonia, Claude Fischer, Eric Bazile, François Bouyssel, Radmila Brožková, Pierre Bénard, Bogdan Bochenek, Daan Degrauwe, Maria Derkova, Ryad El Khatib, Rafiq Hamdi, Ján Ma?ek, Patricia Pottier, Neva Pristov, Yann Seity, Petra Smolíková, Oldrich Spaniel, Martina Tudor, Yong Wang, Christoph Wittmann, and Alain Joly, 2017: The ALADIN System and its Canonical Model Configurations AROME and ALARO, 2017, Geoscientific Model Development, submitted.

Thompson, G., P. R. Field, et al. (2008). "Explicit Forecasts of Winter Precipitation Using an Improved Bulk Microphysics Scheme. Part II: Implementation of a New Snow Parameterization." Monthly Weather Review 136(12): 5095-5115.

L. Tomassini, P. R. Field, R. Honnert, S. Malardel, R. McTaggart-Cowan, K. Saitou, A. T. Noda, and A. Seifert (2017), The "Grey Zone" cold air outbreak global model intercomparison: A cross evaluation using large-eddy simulations, J. Adv. Model. Earth Syst., 9, doi: 10.1002/2016MS000822

Váňa, F., P. Bénard, J.-F. Geleyn, A. Simon and Y. Seity, 2008:Semi-Lagrangian advection scheme with controlled damping: An alternative to nonlinear horizontal diffusion in a numerical weather prediction model. Quart. J. Roy. Meteorol. Soc., 134, 523-537.

Walters, D., I. Boutle, et al. (2017). "The Met Office Unified Model Global Atmosphere 6.0/6.1 and JULES Global Land 6.0/6.1

configurations." Geoscientific Model Development 10(4): 1487-1520.

Wayland R.J. and Raman S., 1994: Structure of the marine atmospheric boundary layer during two cold air outbreaks of varying intensities: GALE 86. Boundary-Layer Met., 71, 43-66.

Wentz, FJ and Spencer, RW, 1998. SSM/I rain retrievals within a unified all-weather ocean algorithm. Journal of the Atmospheric Sciences, 55, 9, 1613-1627, 10.1175/1520-0469(1998)055<1613:SIRRWA>2.0.CO;2

Wielicki, B. A., B. R. Barkstrom, E. F. Harrison, R. B. Lee III, G. L. Smith, and J. E. Cooper, 1996:Clouds and the Earth's Radiant Energy System (CERES): An Earth Observing System Experiment, Bull. Amer. Meteor. Soc., 77, 853-868.

Wilkinson, J. M., H. Wells, et al. (2013). "Investigation and prediction of helicopter-triggered lightning over the North Sea." Meteorological Applications 20(1): 94-106.

Wilson, D. R. and S. P. Ballard (1999). "A microphysically based precipitation scheme for the UK Meteorological Office Unified Model." Quarterly Journal of the Royal Meteorological Society 125(557): 1607-1636.

Wyngaard, J. C. (2004). "Toward numerical modeling in the "terra incognita"." Journal of the Atmospheric Sciences 61(14): 1816-1826.

Xu, K. M. and D. A. Randall (1996). "A semiempirical cloudiness parameterization for use in climate models." Journal of the Atmospheric Sciences 53(21): 3084-3102.

Yueyue Yu, Rongcai Ren, and Ming Cai, 2015: Dynamic Linkage between Cold Air Outbreaks and Intensity Variations of the Meridional Mass Circulation. J. Atmos. Sci., 72, 3214-3232.

a) Met Office analysis chart for 12Z 31st January 2010. b) MODIS image (channel 4, 550nm) for midday 31st January 2010. The blue square indicates the stratocumulus region and the orange box indicates the convective region. The larger yellow box indicates the region used for the rainrate plot in fig. 7. c) Schematic of the cloud evolution as the air sweeps down over the course of $\sim$ 12 hours from the north (left) to the south (right), indicating cloud morphology and gross properties including hydrometeor concentrations, windspeed, boundary layer height and total sensible plus latent heat flux. Sea ice extent from http://igloo.atmos.uiuc.edu

Top of atmosphere outgoing longwave fluxes from models from a 24 hour forecast valid for 12UTC 31 January 2010. Each row shows from left to right, 1km convection off, 1 km convection on, 16km convection off, 16 km convection on (except AROME which is 4km instead of 16km for lowest resolution). Each row is a different model indicated in the panel.

Same as fig 7

Same as fig 7

Area mean values in the 100km x 100km stratocumulus region from the convection off simulations as a function of resolution for a) longwave outgoing top of atmosphere flux b) shortwave outgoing top of atmosphere flux. The satellite derived estimates are given as a whisker plot (5,25,mean,75,95 percentiles). The horizontal bars at the top of the panels indicate the average, across the resolutions, of 2 standard deviations derived from the 100km box

Same as fig 7, but with a) liquid water path, b) ice water path.

Same as fig 7, but with convection-ON.

Same as fig 7, but with convection-ON.

Mean profiles for the stratocumulus region for 16km resolution simulations (a,b) and 1km simulations (c,d). Potential temperature (a,c) and total water (b,d) are shown. Solid is for convection off, while dashed is convection on.

Same as fig 7, but for convective region.

Same as fig 7, but for convective region.

Same as fig 7, but for convective region.

Same as fig 7, but for convective region.

Same as fig 7, but for convective region.The solid circles with error bars are from aircraft measurements and the solid black lines are data from dropsondes (See Field et al. 2014)

Mean profiles for the convective region for 1km resolution simulations. a) total liquid, b) total ice. Solid circles represent aircraft observations and the lines represent the interquartile range for each aircraft leg.

Mean hourly accumulated rain as a function of resolution from three 10 min accumulations at 1050-1100,1150-1200,1250-1300 for the region in the convective part of the domain depicted in fig. 7.Solid lines: convection-off simulations, dashed line: convection-on simulations.

.

vertical wind distributions for the stratocumulus region at 1km for convection-off (solid) and convection-on (dash) simulations. The thinnest line is the lowest resolution, the thickest line is the highest resolution.

Same as figure 7 except for convective region

Exploring the convective grey zone with regional simulations of a cold air outbreak

Paul R. Field*, Radmila Brožková, Ming Chen, Jimy Dudhia, Christine Lac, Tabito Hara, Rachel Honnert, Joe Olson, Pier Siebesma, Stephan de Roode, Lorenzo Tomassini, Adrian Hill , Ron McTagart-Cowan

Nine regional models have been used to simulate a cold air outbreak for a range of grid spacings (1km to 16km) with parametrized convection off or on. There is more spread between model results for the simulations in which convection is parametrized when compared to simulations in which convection is represented explicitly. The stratocumulus region is not well reproduced by the models, which tend to predict open cell convection. For the convective region the model spread reduces with increased resolution.

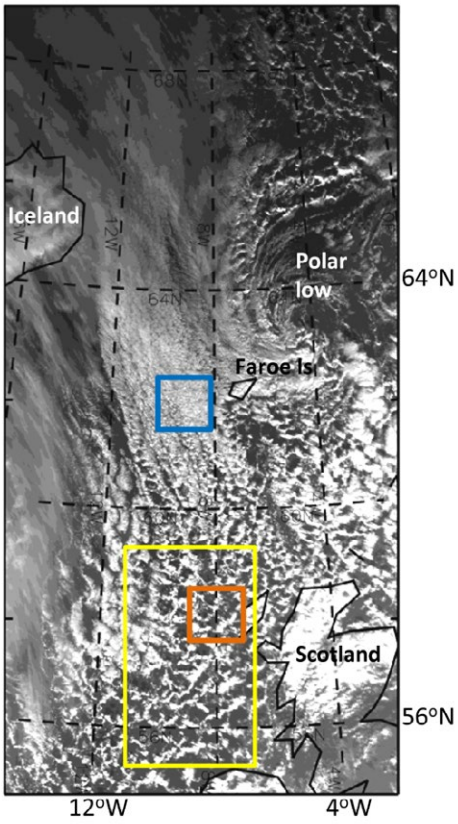

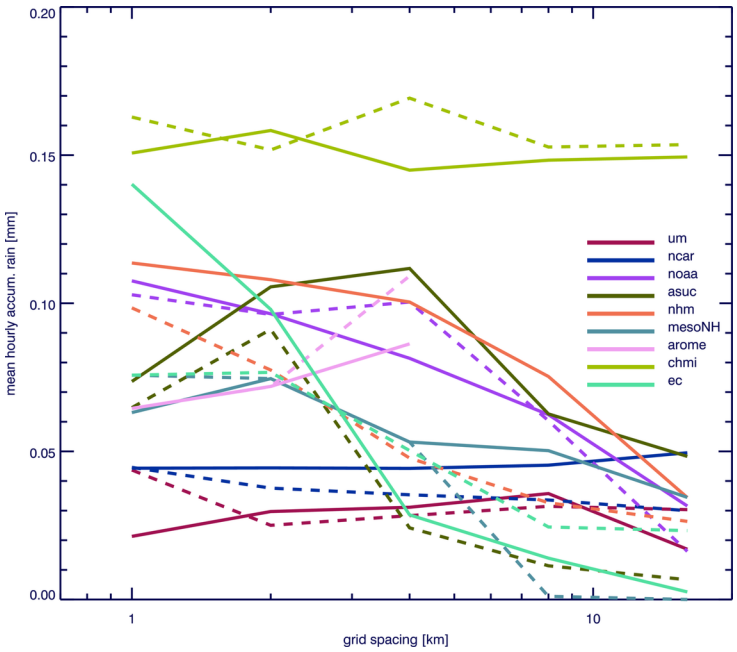

greyzone_plot_precip_hist1.png

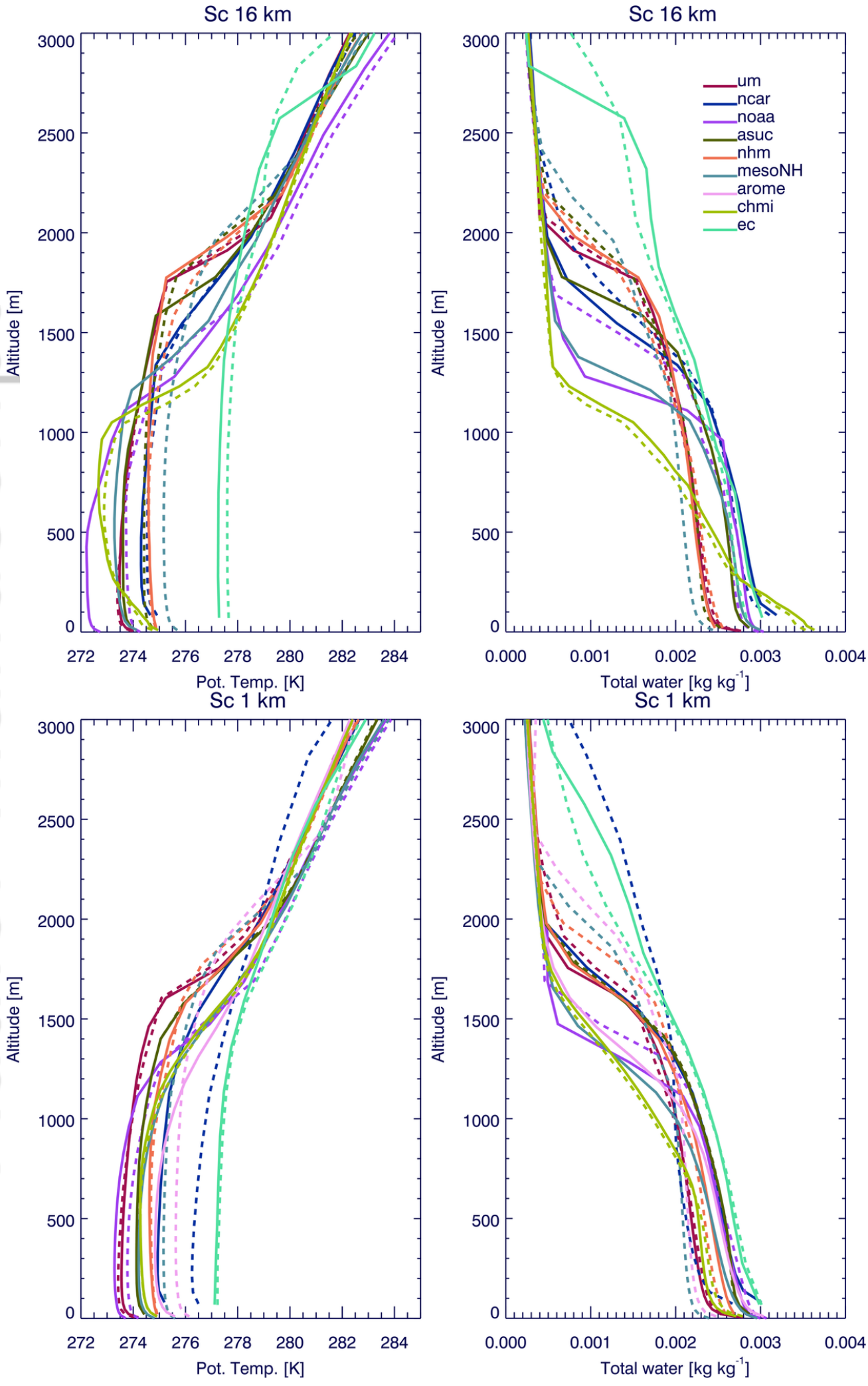

greyzone_plot_profile1.png

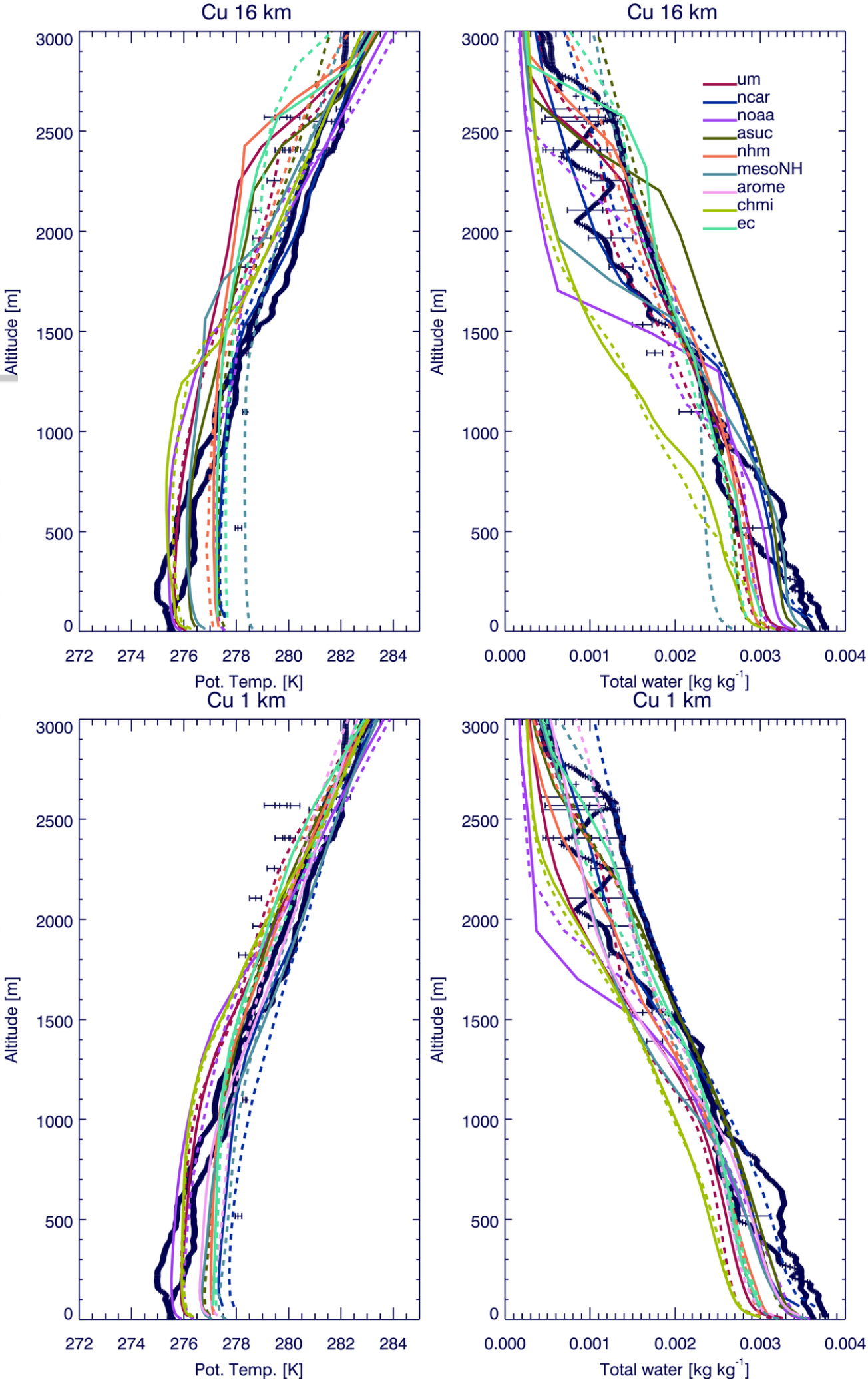

greyzone_plot_profile2.png

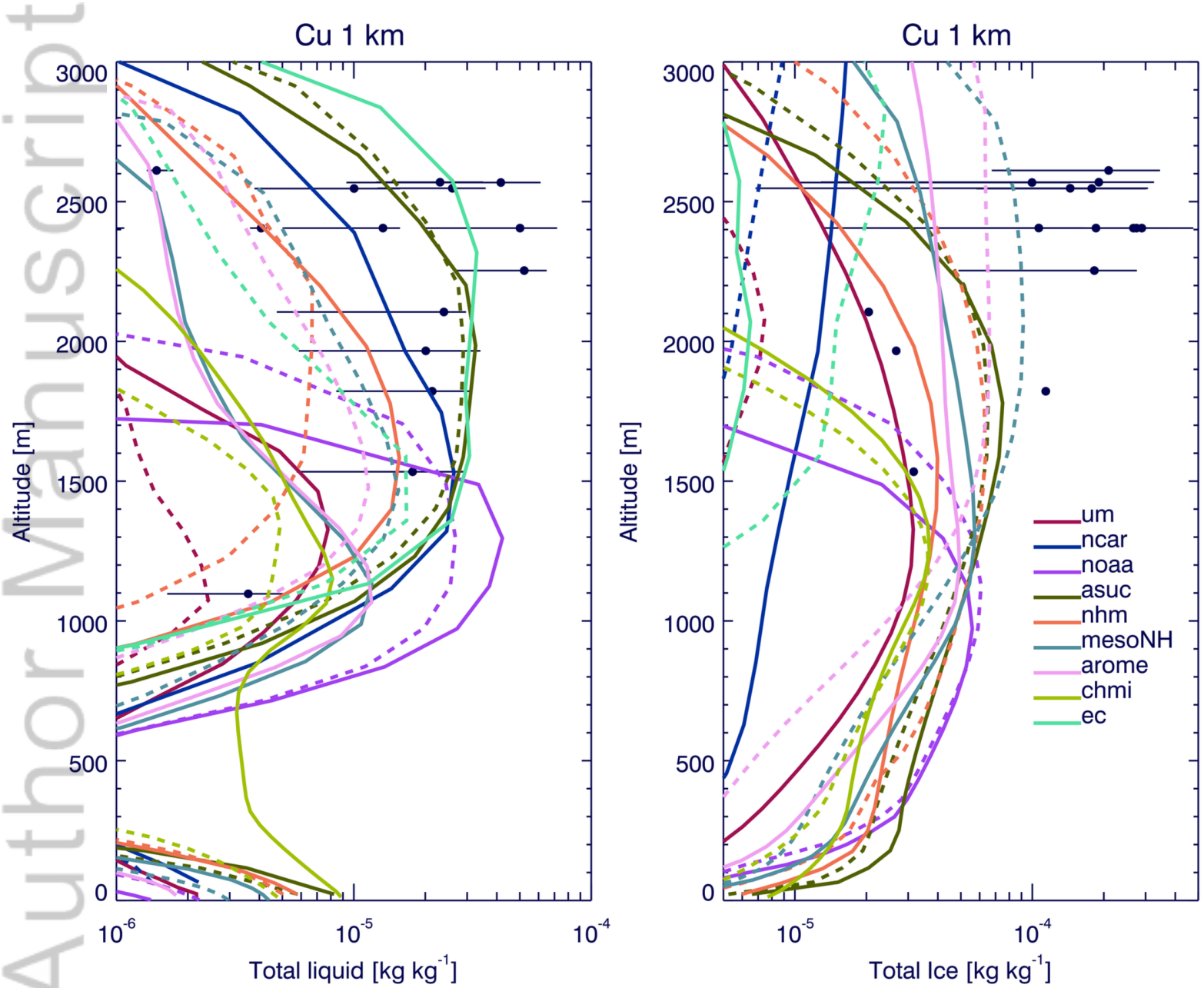

greyzone_plot_profile3.png

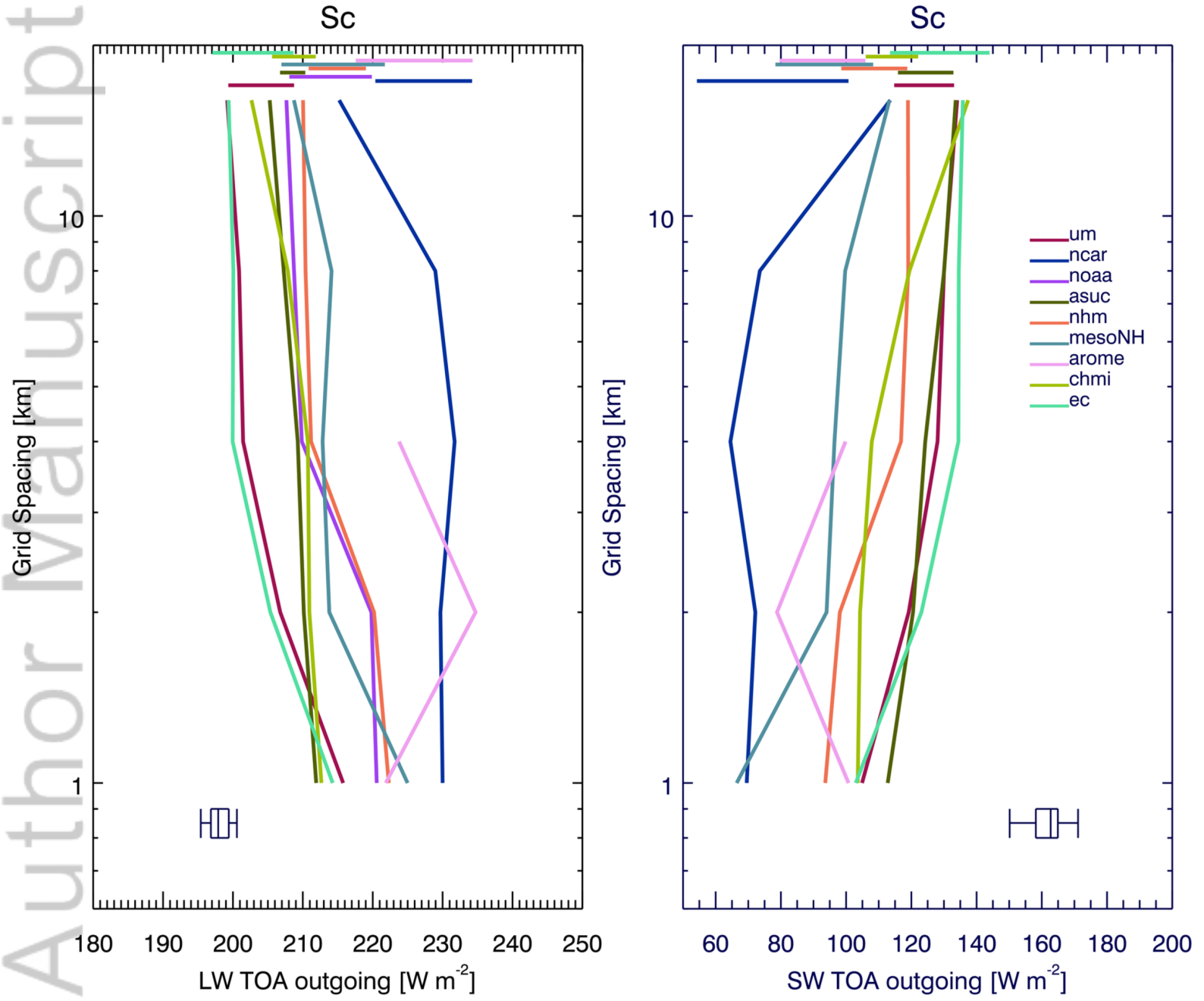

greyzone_plot_surface_means1.png

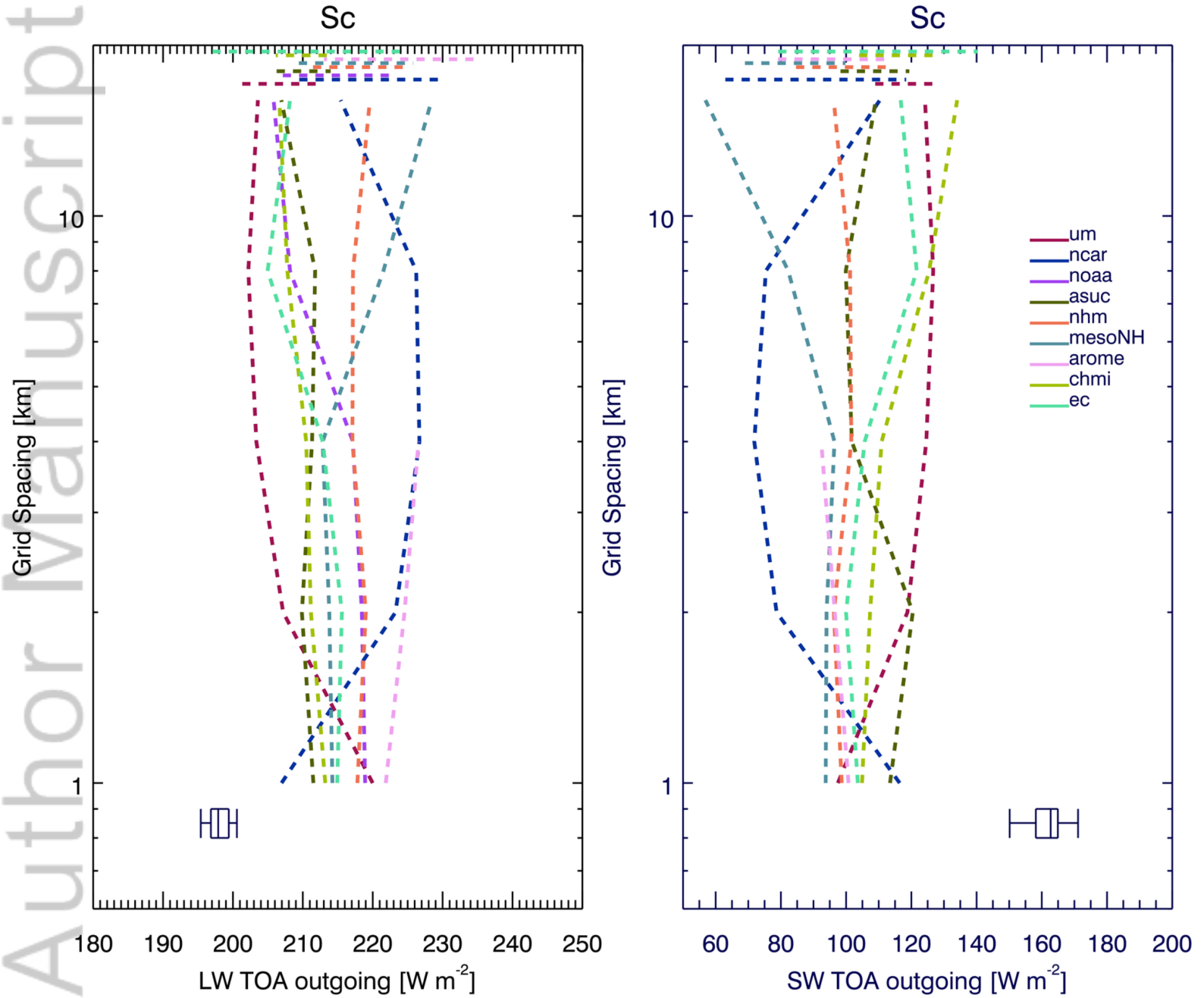

greyzone_plot_surface_means1convon.png

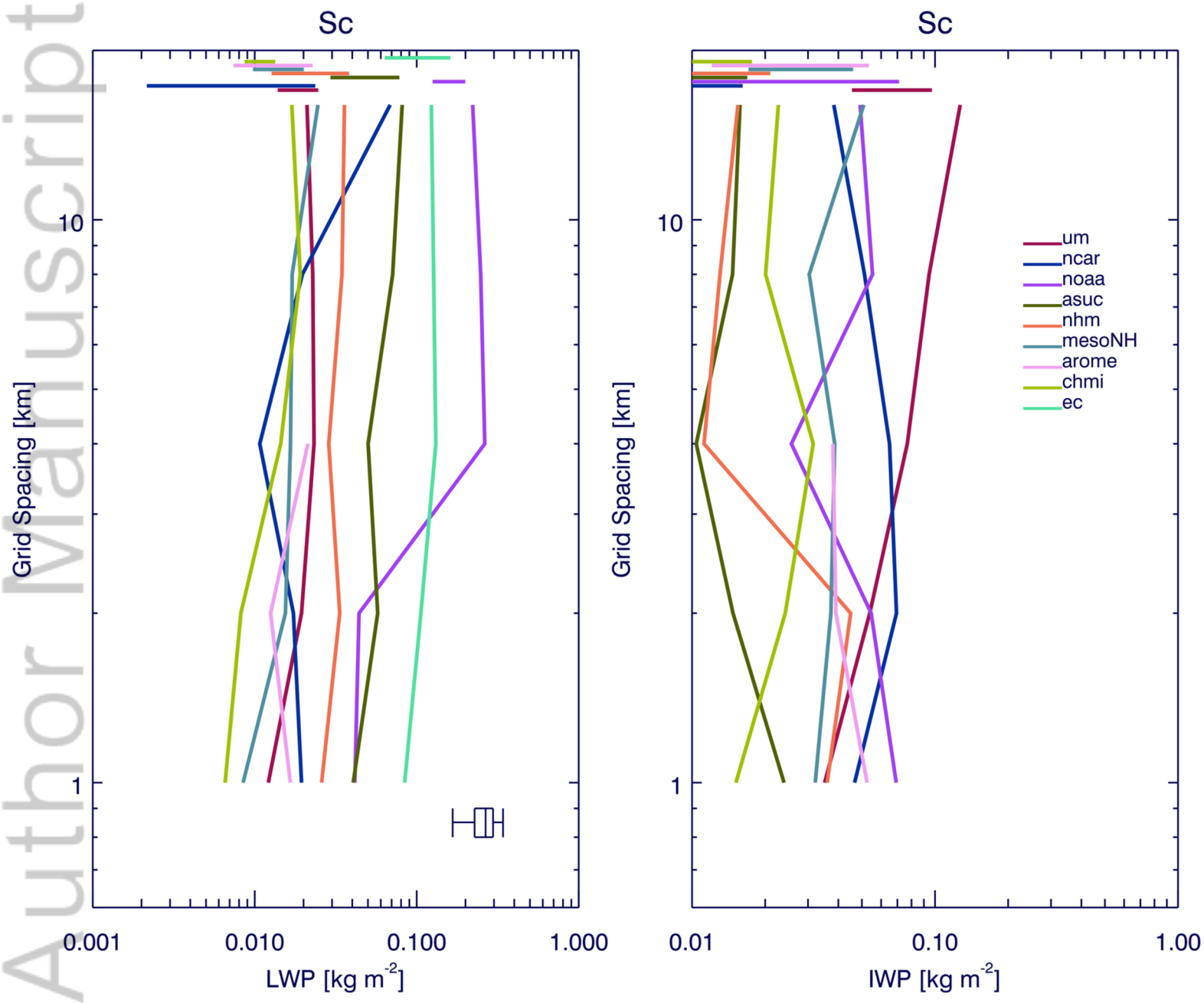

greyzone_plot_surface_means2.png

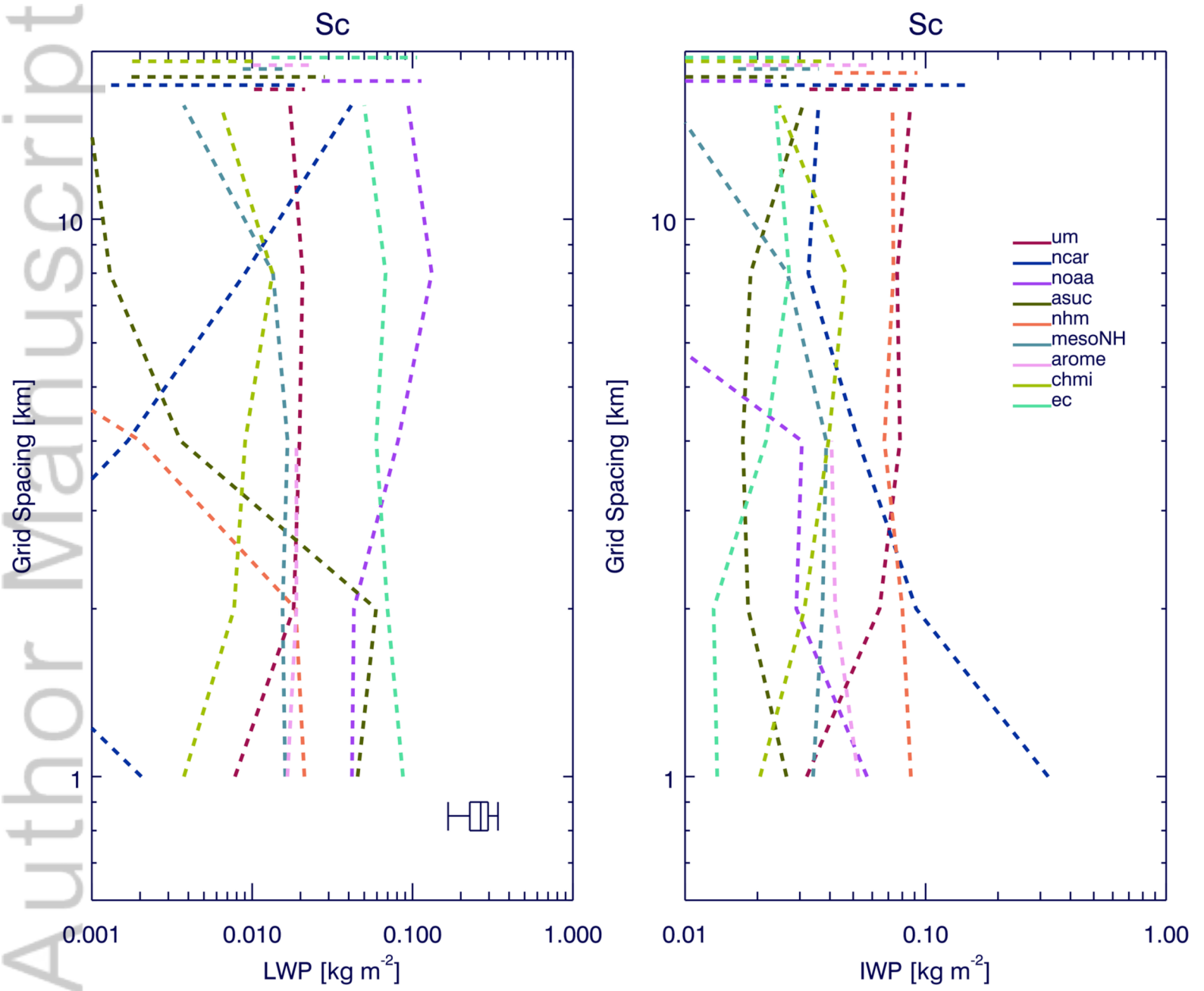

greyzone_plot_surface_means2convon.png

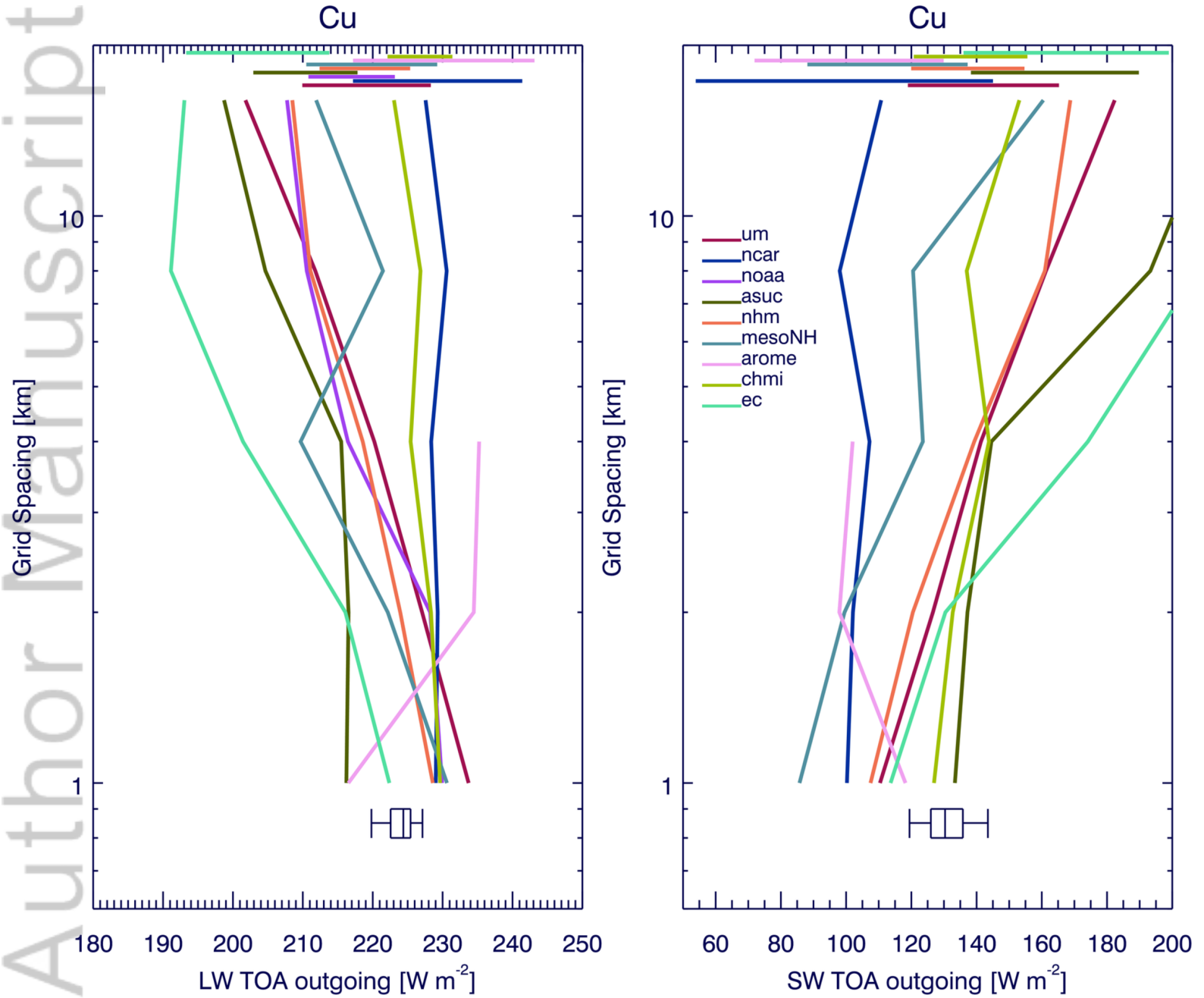

greyzone_plot_surface_means3.png

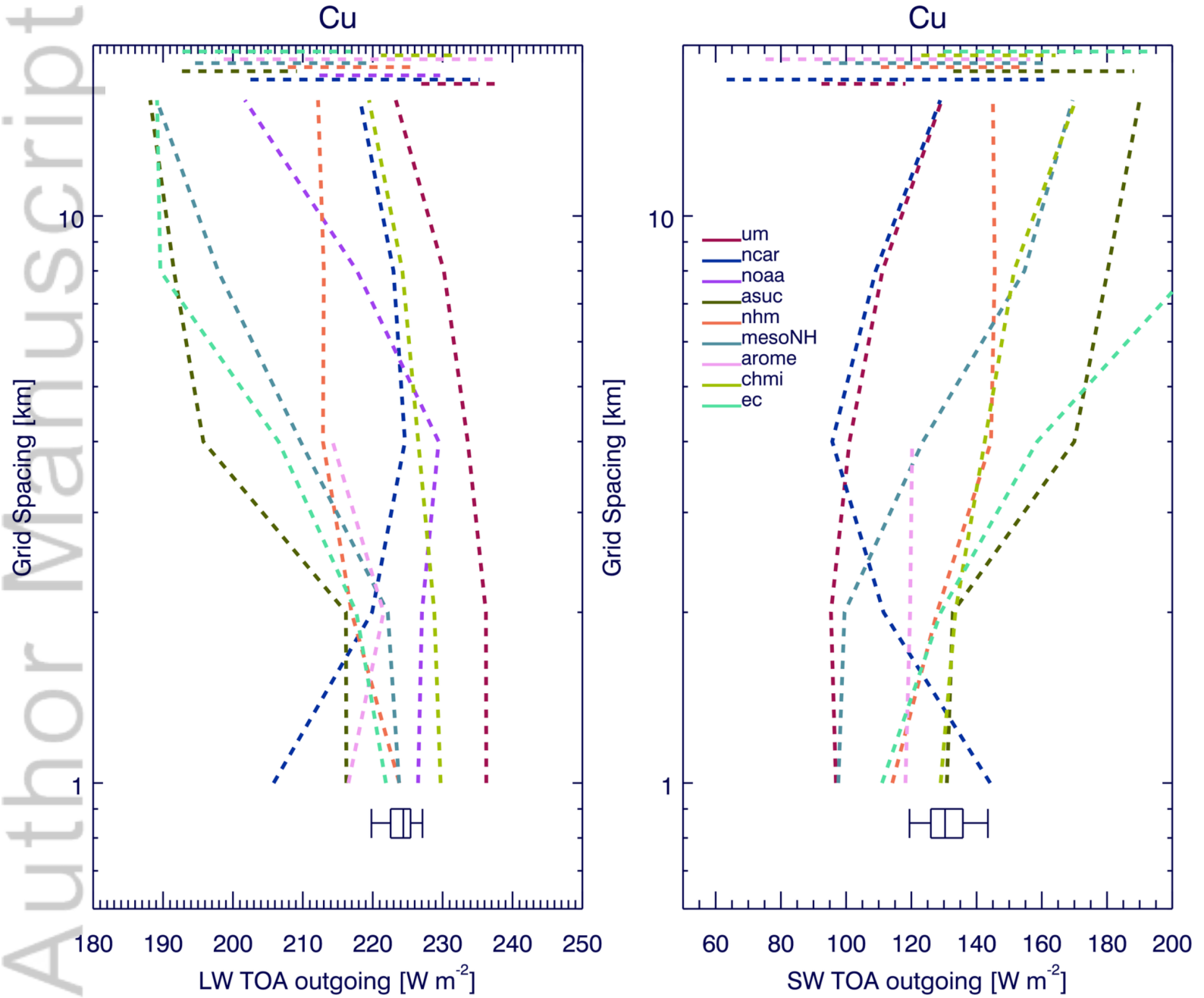

greyzone_plot_surface_means3convon.png

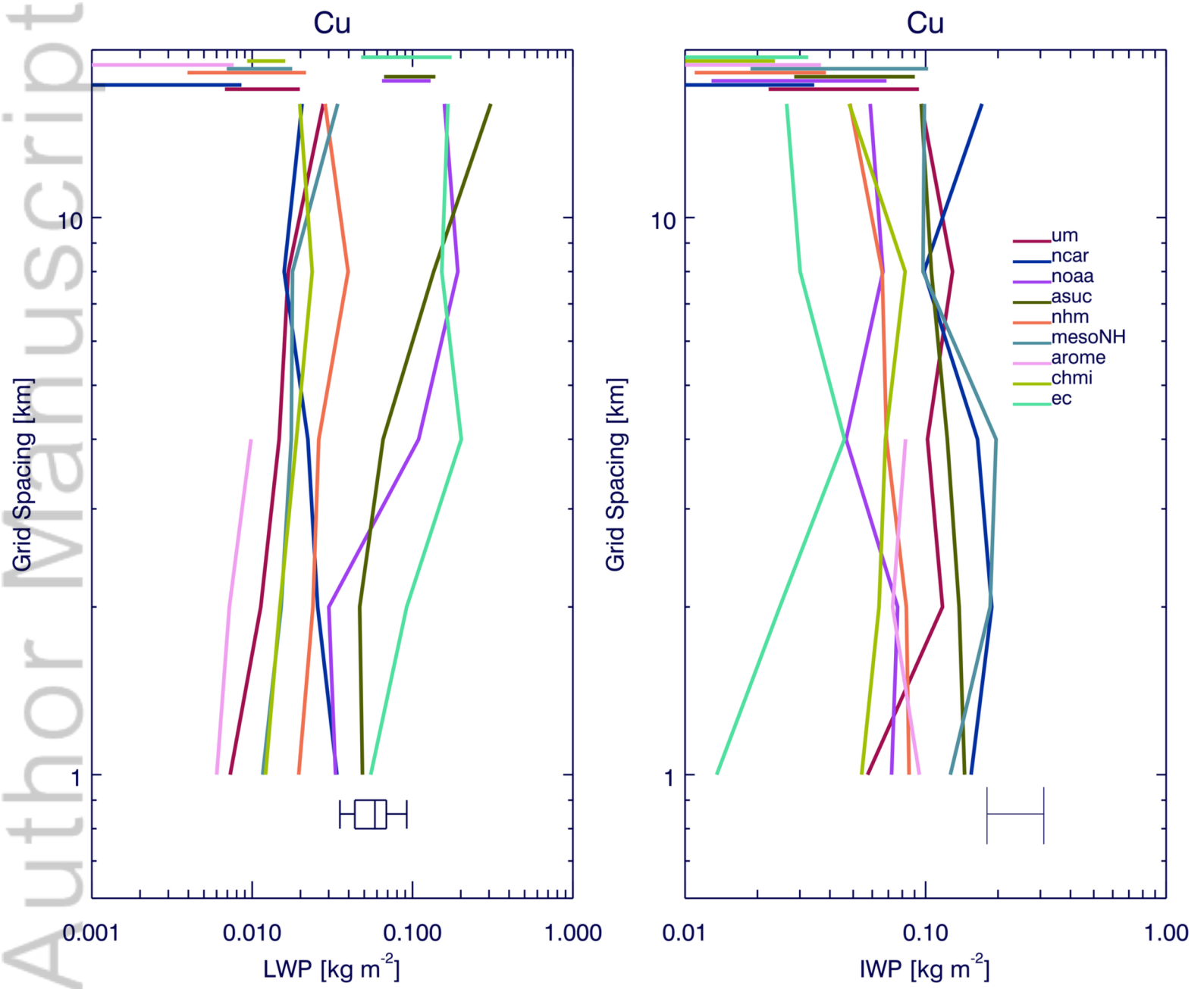

greyzone_plot_surface_means4.png

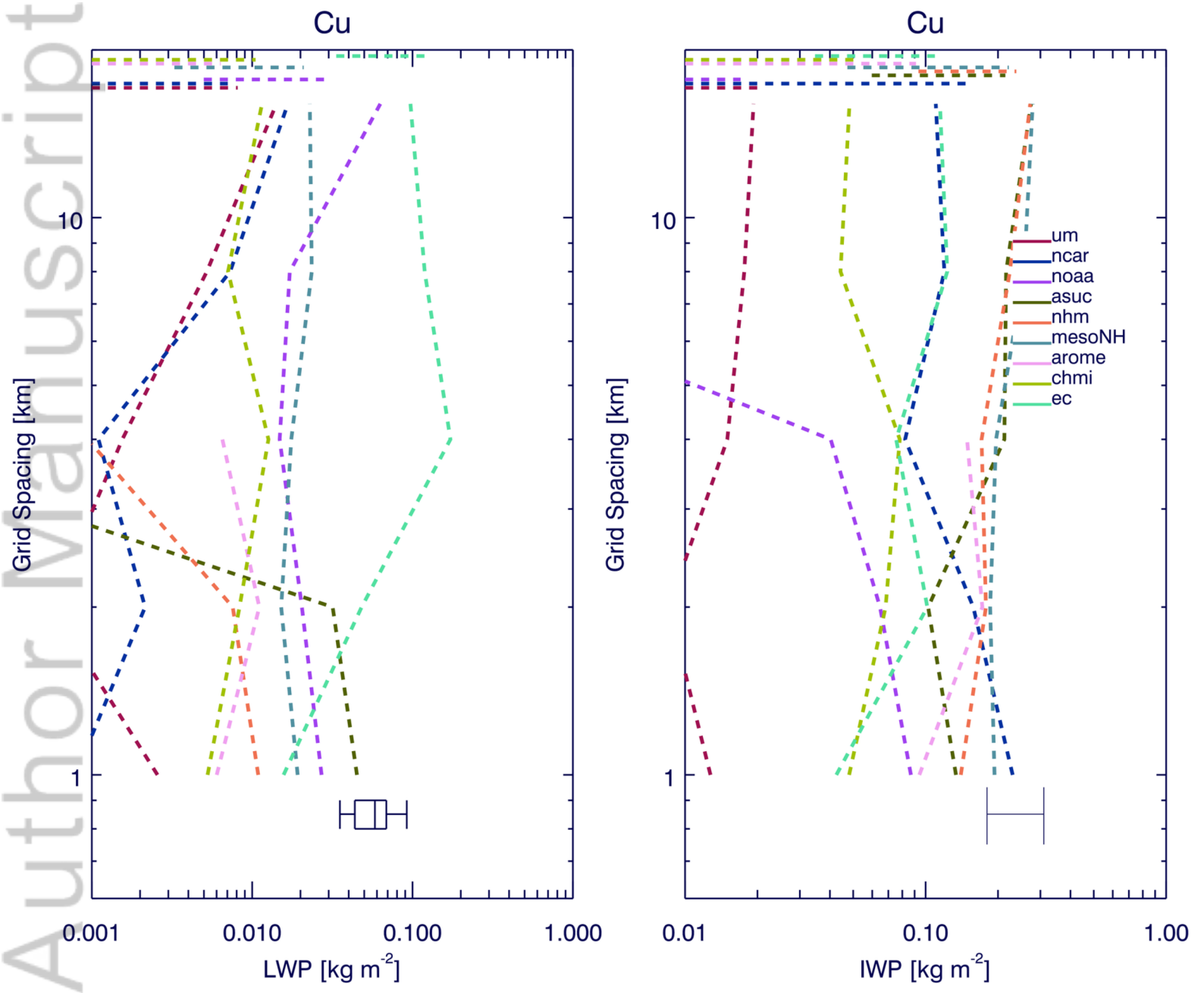

greyzone_plot_surface_means4convon.png

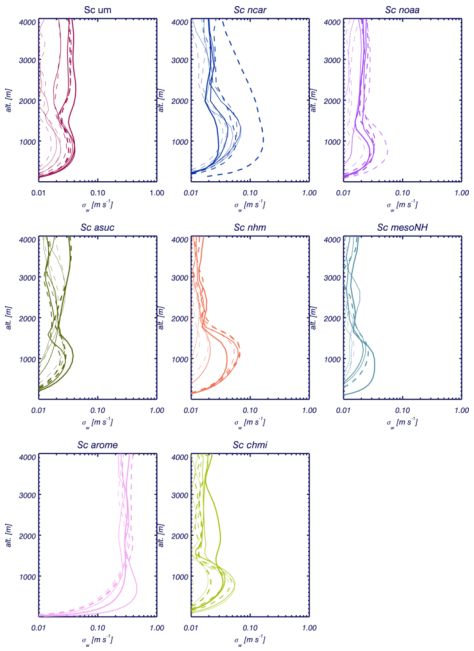

greyzone_plot_w_dist-0.png

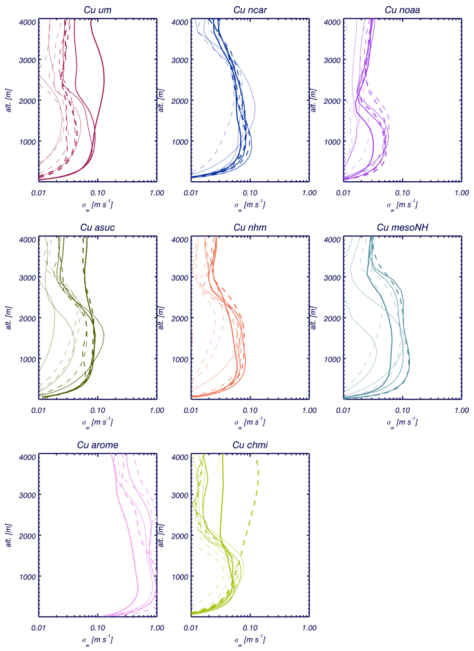

greyzone_plot_w_dist-1.png

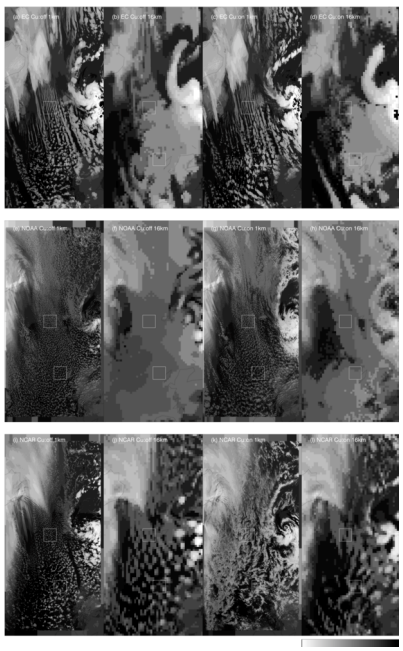

plw0.png

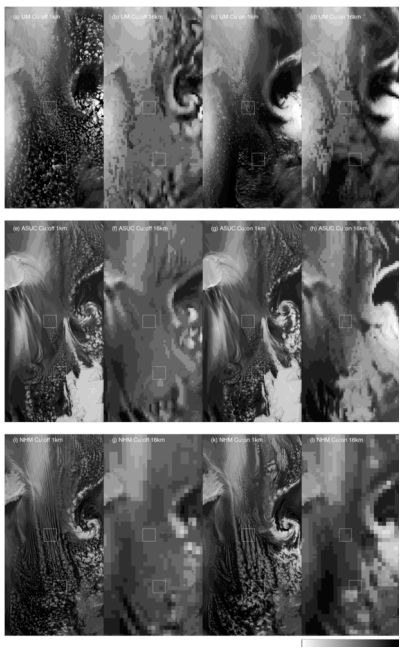

plw1.png

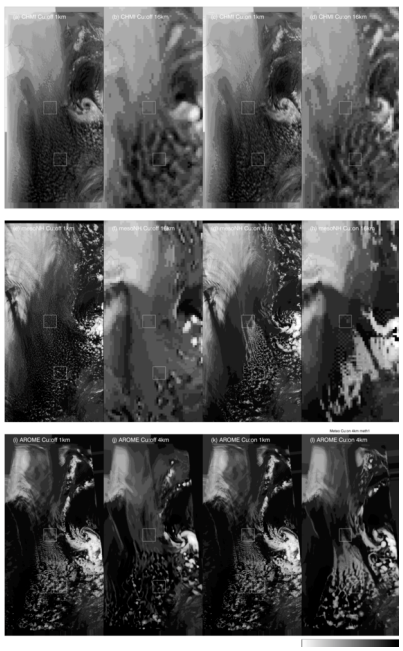

plw2.png

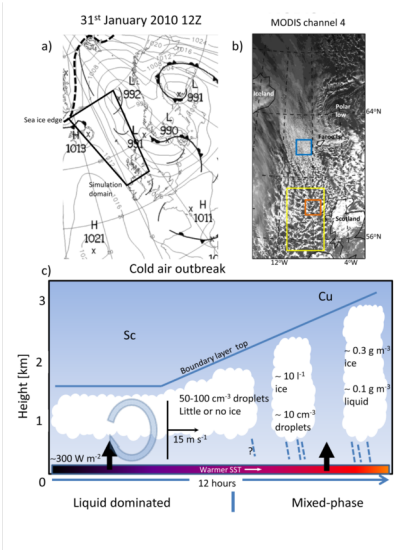

schem.png